JOURNAL OF MATERIALS SCIENCE 17 (1982) 2887–2894

Structural inhomogeneities of AlSi alloys rapidly quenched from the melt

R. DELHEZ, TH. H. DE KEIJSER, E. J. MITTEMEIJER, P. VAN MOURIK, N. M. VAN DER PERS, L. KATGERMAN, W. E. ZALM
Laboratory of Metallurgy, Delft University of Technology, Rotterdamseweg 137, 2628 AL Delft, The Netherlands

Hypo- and hyper-eutectic AlSi alloys were rapidly quenched from the melt using the melt-spinning technique with two spinning velocities. Structural differences between the wheel (chill) and upper sides of the melt-spun ribbons were investigated by optical and scanning electron microscopy and X-ray diffraction methods (texture- and size-strain analyses). The Al-rich phase of the hypo-eutectic alloys was textured. The textures observed from both sides of the ribbons were different; in neither case was it of fibre type. For the larger spinning velocity applied, the structural imperfection of the wheel side was larger than that of the upper side for both the Al-rich and the Si-rich phases.

1. Introduction

By rapid quenching from the melt, recycling of scrap material may be facilitated because the solid solubility of alloying elements is enlarged and/or a very fine structure is developed [1]. A considerable part of the aluminium scrap consists of alloys with silicon as major alloying element.

It was shown recently [2], that considerable variations in the metastable solid solubility of silicon in aluminium occur as a function of ribbon thickness. Also in view of a possible commercial application of the melt-spinning process, the former analysis is extended to a description of the preferred orientations and micro-structure (size-strain analysis) of the aluminium and silicon phases present at the wheel (chill) and upper sides of the ribbons.

2. Experimental details

2.1. Specimen preparation

Aluminium–silicon alloys with compositions 0, 2.5, 12.6 and 33.9 at% Si were prepared from 99.998 wt% Al and 99.99 wt% Si by melt-spinning (i.e. impinging a jet of molten alloy onto the cylindrical surface of a rotating copper wheel) as described previously [2]. The ribbons obtained were irregular varying in thickness from ~0.1 (not only at the edges) to 150 μm. Therefore, no useful information was available for the average thickness.

2.2. Metallography

Optical and scanning electron microscopy were performed with a Neophot-2 (Carl Zeiss Jena) optical microscope and a Jeol JXA-50A scanning electron microscope, respectively. Wheel and upper sides and cross-sections of the ribbons were examined after mechanical polishing and etching in a 5 or 10% KOH solution or Keller and Wilcox's reagent. Applying an accelerating voltage of 20 kV, SEM micrographs were obtained from specimens covered with a vacuum-deposited gold layer to enhance contrast.

2.3. X-ray diffraction

Specimens for the X-ray diffraction analysis were composed of a number of ribbons (as much as possible of uniform and equal thickness in the range 20–150 μm) placed parallel to each other with either wheel or upper side at the surface.

2.3.1. Texture analysis

Pole figures were determined according to the Schulz reflection technique [3] using Co$K\alpha$ radiation and a Siemens Lücke-type texture

0022–2461/82/102887–08$03.46/0

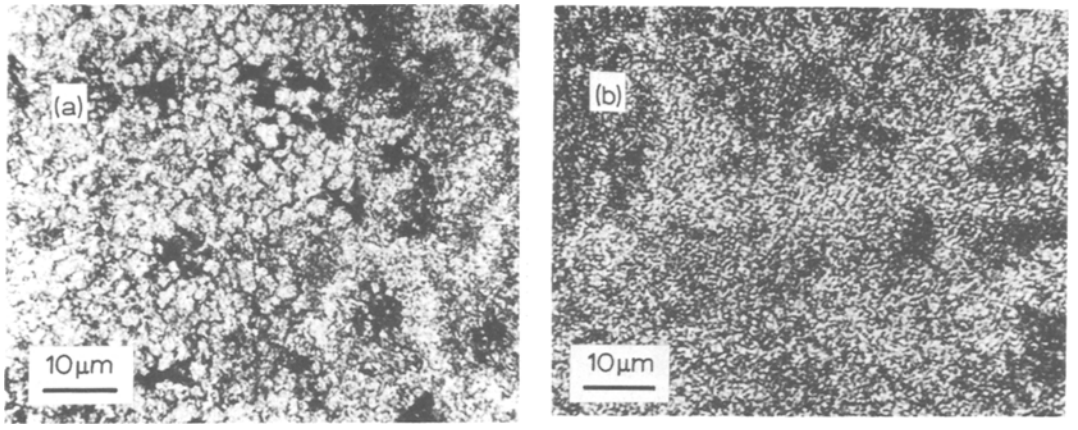

Figure 1 Optical micrographs in the plane of the ribbon of upper side (a) and wheel side (b) of a melt-spun ribbon of the hypo-eutectic AlSi (2.5 at % Si) alloy.

goniometer. The measured intensities were corrected for background radiation and defocusing effects. The pole figures were plotted according to Love [4]. The low-angle reflections 1 1 1 and 2 0 0 were used, because then the X-rays penetrate least into the specimen and discrimination between wheel and upper side is optimal.

2.3.2. Line profile analysis

Line profiles from the aluminium-rich and silicon-rich phases were recorded with Co$K\alpha$ radiation. A Siemens type F ω-diffractometer was used, having a graphite monochromator in the diffracted beam and operating at low scanning speed to obtain sufficient counting accuracy. Large portions of the background at both sides of the peaks were recorded. The background was interpolated linearly between the two extremities. For the elimination of the α_2 component [5] the ratio R (where $R = I\alpha_2(\max)/I\alpha_1(\max)$ and $I\alpha_1$ and $I\alpha_2$ are the intensities of the α_1 and α_2 components, respectively) was taken from a high-angle reflection of the standard specimen.

The broadening due to the instrumental aberrations and the X-ray spectrum used was eliminated with the aid of line profiles recorded from a thin silicon standard specimen (prepared as described in [6]). For analysis of the profiles of the aluminium-rich phase, an interpolation was performed on the 2θ-scale between the breadths of the reflections of this silicon standard.

3. Results

3.1. Morphology

Optical micrographs characteristic of the upper and wheel sides of the hypo-eutectic AlSi (2.5 at %

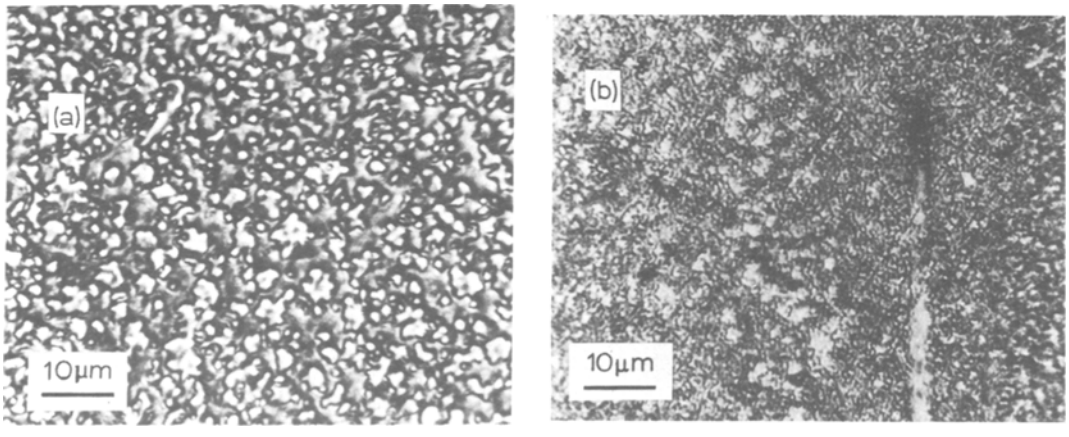

Figure 2 Optical micrographs in the plane of the ribbon of upper side (a) and wheel side (b) of a melt-spun ribbon of the hyper-eutectic AlSi (33.9 at % Si) alloy.

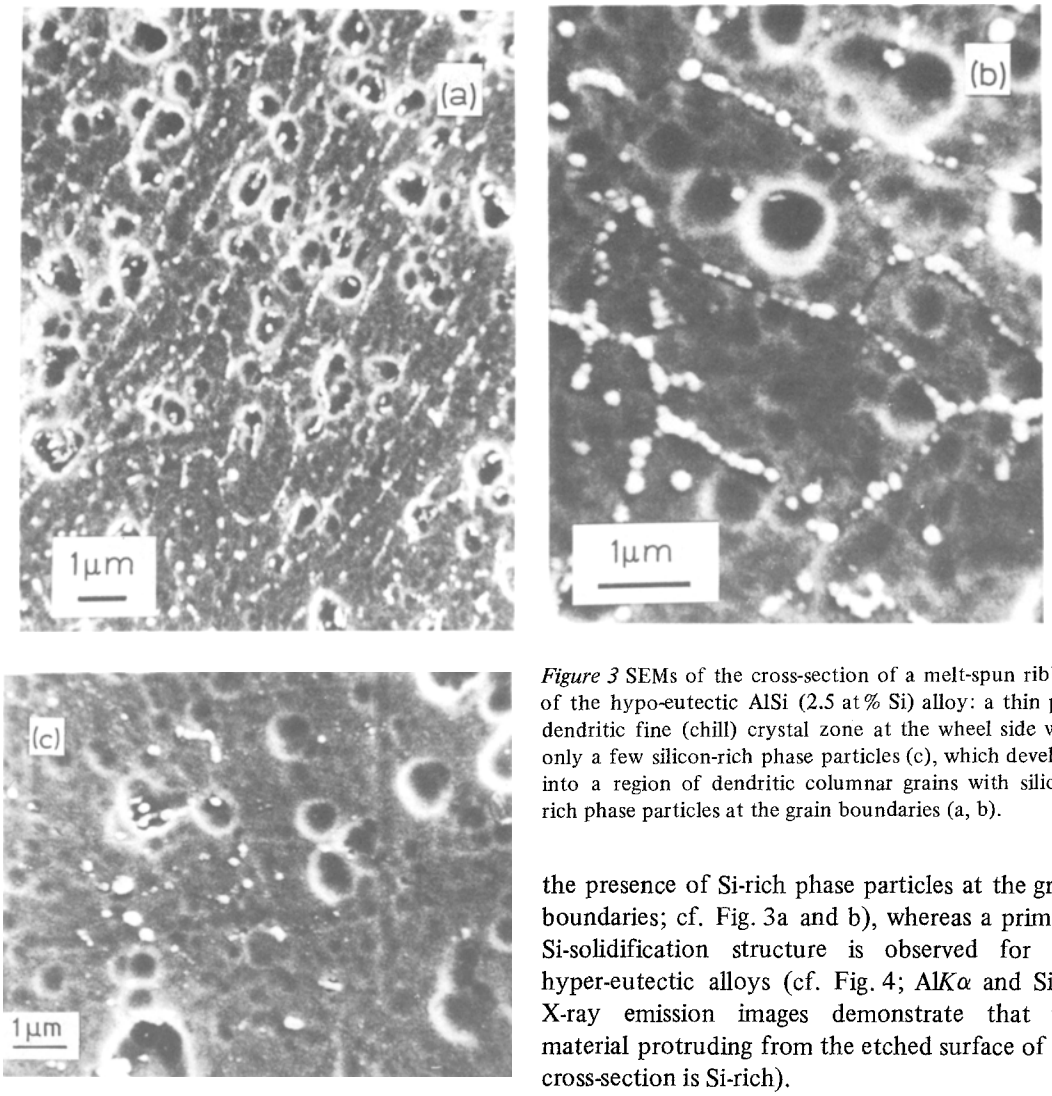

Figure 3 SEMs of the cross-section of a melt-spun ribbon of the hypo-eutectic AlSi (2.5 at% Si) alloy: a thin predendritic fine (chill) crystal zone at the wheel side with only a few silicon-rich phase particles (c), which develops into a region of dendritic columnar grains with silicon-rich phase particles at the grain boundaries (a, b).

Si) and the hyper-eutectic AlSi (33.9 at% Si) alloys were obtained after very slight mechanical polishing and subsequent etching (Figs 1a, b and 2a, b). It can be seen that the structure at the upper side is considerably coarser than at the wheel side.

Optical and SEM micrographs of the cross-sections show that, especially at those places where the absence of curvature at the wheel side indicates good contact between wheel and ribbon during solidification, a thin fine-grained region with only a few silicon-rich phase particles is adjacent to the wheel–ribbon interface ("featureless" zone: e.g. Fig. 3c).

On top of this zone, a primary Al-rich solidification structure is observed for the hypo-eutectic alloy (a region of columnar grains as suggested by the presence of Si-rich phase particles at the grain boundaries; cf. Fig. 3a and b), whereas a primary Si-solidification structure is observed for the hyper-eutectic alloys (cf. Fig. 4; Al$K\alpha$ and Si$K\alpha$ X-ray emission images demonstrate that the material protruding from the etched surface of the cross-section is Si-rich).

3.2. Preferred orientations

The silicon-rich phase did not show any preferred orientation.

With reference to the surface and the axis of a ribbon, the texture of the aluminium-rich phase in hypo-eutectic alloys can be described as follows:

wheel side: {1 1 0} ⟨1 0 0⟩;

upper side: {1 0 0} ⟨1 1 0⟩.

Examples of 1 1 1-pole figures for the AlSi (2.5 at% Si) alloy are shown in Fig. 5a and b. The 2 0 0-pole figures were also determined and gave results consistent with the 1 1 1-pole figures.

The textures are symmetrical with respect to the longitudinal section. Furthermore, it is seen that the texture of the upper side shows an "off-

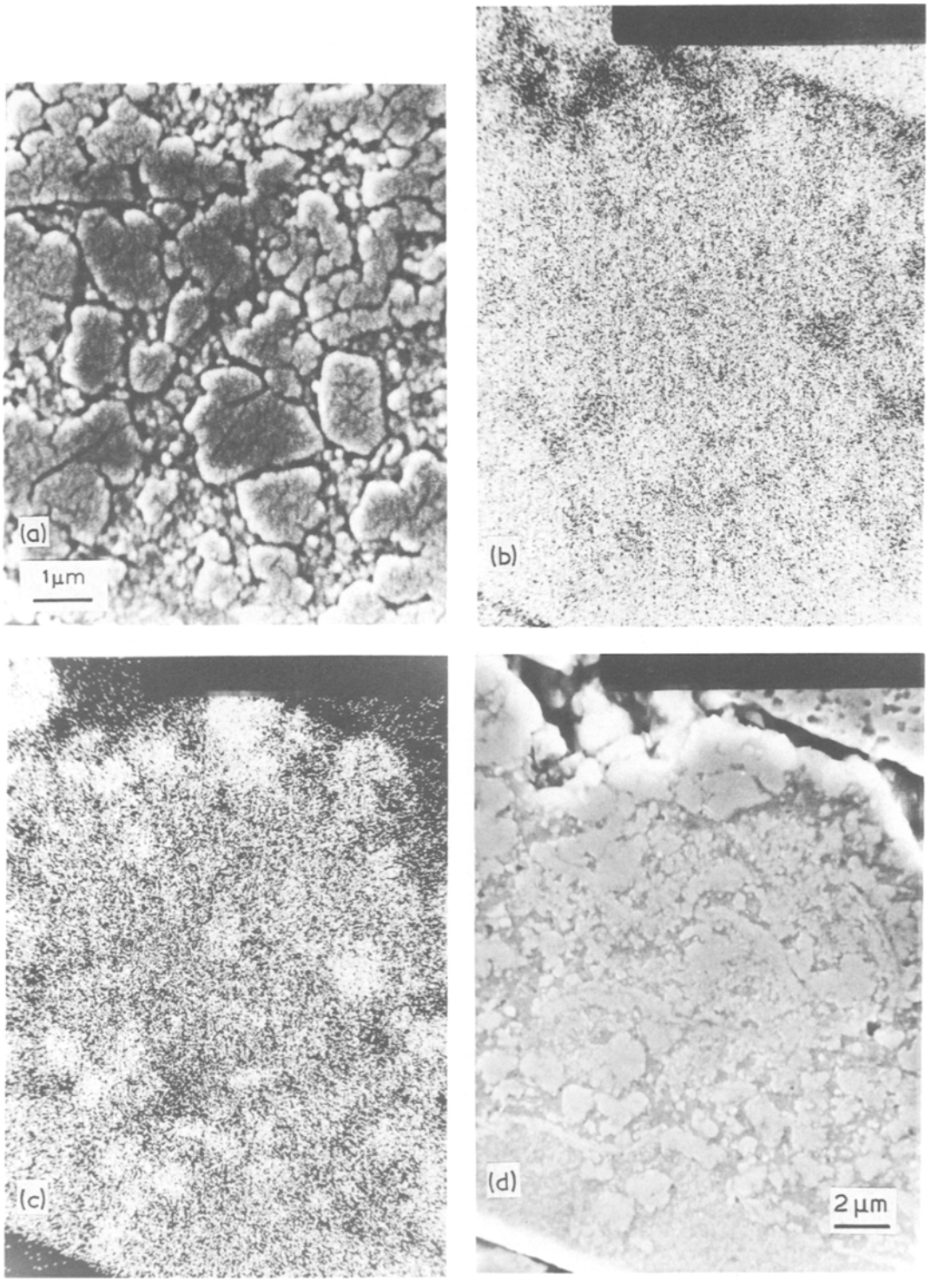

Figure 4 SEM of the cross-section of a melt-spun ribbon of the hyper-eutectic AlSi (33.9 at% Si) alloy showing a primary silicon-rich phase (facetted) solidification structure (a). The Al$K\alpha$ and Si$K\alpha$ X-ray emission images (b and c; d is the corresponding electron image) demonstrate that the material protruding from the etched surface is Si-rich.

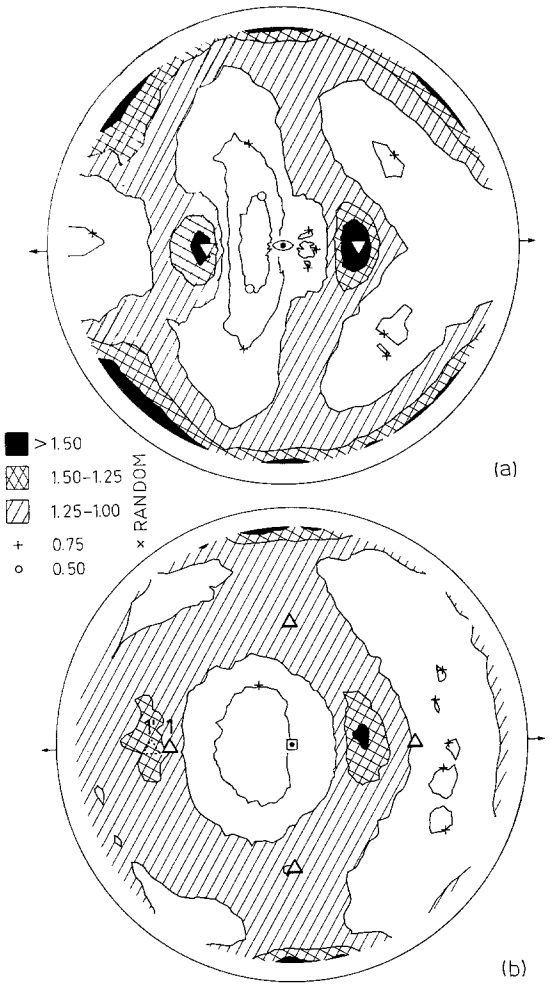

Figure 5 1 1 1-pole figures of the aluminium-rich phase present at the wheel side (a) and the upper side (b) of melt-spun ribbons of the hypo-eutectic AlSi (2.5 at% Si) alloy. The ribbon axis is indicated by the arrow. The single-crystal orientation designating the preferred orientation observed is indicated. Note the "off-set" for the texture of the upper side as indicated by the difference between for example the positions 1 and 1′.

set" of about 5–10° with respect to the preferred orientation indicated above (note the difference between, for example, the positions 1 and 1′ in Fig. 5b).

Because of the penetration of the X-rays, in the pole figure obtained from one side of the ribbon some phenomena of the pole figure of the other side could be observed too. This effect was stronger for the wheel side than for the upper side. Therefore, it is concluded that the preferred orientation of the wheel side is restricted to a smaller part of the ribbon thickness than the preferred orientation of the upper side.

TABLE I The ratio R of the difference between the maximum and the minimum intensities observed in the 1 1 1-pole figures of the aluminium-rich phase in melt-spun AlSi alloys and the intensity which would be observed from a specimen without preferred orientation

Silicon content (at.%)	Circumferential velocity (m sec^{-1})	R	
		Upper side	Wheel side
0	38.6	2.5	1.8
12.6	23.2	1.5	1.5
12.6	46.2	1.2	1.2
33.9	46.2	0.8	0.7

With increasing silicon content of the alloy and increasing circumferential velocity of the wheel, the sharpness of the texture of the aluminium-rich phase decreased, in particular for the upper side of the ribbons. This may be illustrated roughly by the decrease of the difference between the maximum and minimum intensities observed in the 1 1 1-pole figures from either side (Table I). In the hypereutectic alloy practically no texture is present.

3.3. Crystallite size and lattice strain

The crystallite (domain) sizes and the lattice distortions in the aluminium-rich and the silicon-rich phases can be determined by X-ray diffraction line profile analysis. In this paper, a recently developed single-line method is applied [7]. It was justified that the method is valid for the specimens considered here [7]. All line profiles are assumed to be Voigt functions, i.e. convolutions of Cauchy and Gaussian functions. From the profile to be investigated the integral breadths of the Gaussian and Cauchy components of the only structurally broadened profile are obtained. In practice, size broadening is often considered to result into Cauchy-shaped profiles, whereas strain broadening gives rise to Gaussian-shaped profiles [8, 9]. Then one can apply for the determination of size and strain effects [7]:

$$D_{\mathrm{eff}} = \lambda/\beta_{\mathrm{c}}^{\mathrm{f}} \cos\theta \quad \text{and} \quad e = \beta_{\mathrm{g}}^{\mathrm{f}}/4 \tan\theta,$$

where D_{eff} and e denote the effective crystallite size perpendicular to the reflecting planes and an average microstrain, respectively. $\beta_{\mathrm{c}}^{\mathrm{f}}$ and $\beta_{\mathrm{g}}^{\mathrm{f}}$ are the integral breadths of the Cauchy and Gaussian components of the only structurally broadened profile, f.

The aluminium-rich phase showed a dominant strain broadening: the Cauchy components of the standard profile and the instrumentally and struc-

TABLE II Size-strain analysis of the aluminium-rich and silicon-rich phases of melt-spun ribbons of the AlSi (12.6 at. % Si) alloy. β^f = total integral breadth of the pure profile f; β_c^f = integral breadth Cauchy component of the pure profile f; β_g^f = integral breadth Gaussian component of the pure profile f; D_{eff} = effective crystallite (domain) size and e = microstrain. The microstrain of the Al-rich phase was calculated from the total integral breadth β^f. $D_{eff} = \infty$ denotes $D_{eff} > 20 \times 10^3$ nm

Reflection	Circumferential velocity (m sec^{-1})	Ribbon side	β^f (° 2θ)	β_c^f (° 2θ)	β_g^f (° 2θ)	D_{eff} (10 nm)	$e \times 10^3$
Aluminium-rich phase							
200	23.2	upper	0.149	0.017	0.138	∞	1.3
		wheel	0.134	0.020	0.121	∞	1.2
200	46.2	upper	0.154	0.031	0.134	∞	1.4
		wheel	0.192	0.052	0.157	∞	1.7
Silicon-rich phase							
220	23.2	upper	0.369	0.170	0.250	680	2.0
		wheel	0.377	0.223	0.215	520	1.8
220	46.2	upper	0.690	0.344	0.447	340	3.7
		wheel	0.846	0.317	0.629	370	5.2

turally broadened profile were equal to within the experimental error. Therefore the microstrain of the aluminium-rich phase was calculated from the total integral breadth of the pure, only structurally broadened, profile. The silicon-rich phase showed both size- and strain-broadening. As an example, results of the AlSi (12.6 at % Si) alloy are gathered in Table II.

The differences between wheel and upper side were investigated for pure Al and AlSi (12.6 at % Si) and AlSi (33.9 at % Si) alloys*. In general, the broadening from the aluminium-rich phase did not show a significantly systematic difference between the wheel and upper sides. The broadening from the silicon-rich phase was significantly larger for the wheel side than for the upper side (in particular for the AlSi (12.6 at % Si) alloy; cf. Table II); in general, at the wheel side a smaller crystallite size and a larger microstrain was found than at the upper side.

A large circumferential velocity of the wheel increased the broadening observed from both the aluminium-rich and silicon-rich phases. This held for the wheel sides in particular (see Table II).

4. Discussion

4.1. Hypo-eutectic alloys

From the differences between the results obtained from wheel and upper sides, a subdivision of the cross-section of the melt-spun ribbon is plausible: (i) a thin zone (say 10 μm) at the wheel (chill) side, where an approximately "diffusionless solidification" [10] occurred (the analogue of the massive transformation [11]). During solidification the supercooling was large enough to permit nucleation and growth of the solid phase without an appreciable solute redistribution; only a few silicon-rich phase particles are observed in this region (Fig. 3c). This predendritic fine (chill) crystal zone develops into (ii) a thick zone of columnar, parallel, dendritic grains. At the grain boundaries of this presumably less rapidly solidified material, silicon-rich phase particles are discerned (interdendritic microsegregation; Fig. 3a and b).

Indications for the occurrence of preferred orientations after liquid quenching were rarely obtained [12, 13]. (In splat-cooled aluminium flakes no preferred orientation was observed [14]). The observation of a definite texture *both* at the wheel side and at the upper side of melt-spun ribbons has not been reported before.

The textures observed are not fibre textures, as one may intuitively expect, but they are symmetrical with respect to the longitudinal section of the ribbon. This hints at the presence of anisotropic temperature gradients and/or mechanical stresses during solidification.

The textures observed at the wheel side and at the upper side can be transformed into each other by a 90°-rotation around a ⟨1 1 0⟩-axis parallel to the outer surfaces of the ribbon and perpendicular to the ribbon axis. Because it was found previously that some of the dendrite boundaries in liquid-quenched material are of the twin

*The effect of the silicon content of the alloy on the line broadening observed was discussed in [2].

type [10], we tried to explain the texture of the upper side with respect to the texture of the wheel side by a multiple twinning operation (e.g. [15]), which proved to be impossible.

For the wheel side of melt-spun ribbons, no texture has been observed previously. For the upper side of melt-spun ribbons of nickel-based superalloys it was noted that columnar dendritic grains were aligned approximately along a ⟨1 0 0⟩-direction [16], in agreement with the present results from the AlSi alloys. Also, in conventionally cast AlSi alloys, a ⟨1 0 0⟩-direction appears to be favoured by the growing dendrites [17].

The observation of an "off-set" of about 5–10° for the texture of the upper side can be considered to be related to the columnar crystals angled backwards to the melt pool (cf. [16]), indicating that the temperature gradient makes an angle of 5–10° with the surface normal (cf. Figs 3a and 5b). This sets an essential difference between melt-spun and splat-cooled material; in the latter case [12] the columnar crystals grow perpendicular to the splat surface.

The (aluminium-rich phase) texture of the upper side, especially, became less sharp as the silicon content of the alloy increased, which may indicate the hindrance of preferred growth by the microsegregated silicon-rich phase particles.

Because in the thin (chill) zone at the wheel side of the ribbons only a very small amount of silicon-rich phase particles is observed, the size-strain data for the silicon-rich phase taken at the wheel side are related mainly to the lower part of the columnar grain region. Also, because of the penetration of the X-rays, the size-strain data for the aluminium-rich phase taken at the wheel side are an average for the thin (chill) zone and the lower part of the columnar grain region.

Several factors contribute to the presence of microstrains in both the aluminium-rich and silicon-rich phases:

(i) because a silicon atom in its own diamond-type lattice occupies a volume 23% larger than in the aluminium f c c lattice, considerable misfit strains will be invoked in both phases. This effect will increase with increasing silicon content;

(ii) microstrains in both phases may result from the temperature gradient present during quenching. This effect will be larger at the wheel side than at the upper side;

(iii) after solidification the two-phase alloy cools down to room temperature resulting in thermal strains due to the large difference between the thermal expansions of both phases [18]. This effect will increase with increasing silicon content;

(iv) concentration variations within (solute clustering) and between the diffracting domains lead to apparent strain values [19].

The smaller crystallite (domain) size of the silicon-rich phase at the wheel side as compared to the upper side is presumably related to the larger cooling rate at the wheel side.

A larger spinning velocity of the rotating wheel will cause a larger cooling and solidification rate. Then a less pronounced texture, a larger microstrain and a smaller crystallite size may be expected, as is observed (cf. Tables I and II).

4.2. Hyper-eutectic alloys

As with the hypo-eutectic alloys the hyper-eutectic alloys also possess a thin "featureless" zone at the wheel side, especially if good contact between ribbon and wheel occurred. On top of this zone the primary silicon phase grew in a facetted manner. A relatively high supercooling is required for this mode of solidification. It may then be expected that a more or less homogeneous and rapid solidification occurs throughout this region. This picture can be consistent with: (i) lattice parameter measurements indicating that a considerable amount of aluminium may be incorporated in the silicon-rich phase of the hyper-eutectic alloys, in contrast with the hypo-eutectic alloys [2]; (ii) the observed absence of texture in the hyper-eutectic alloys.

The cooling rate at the wheel side will have been larger than at the upper side and this can explain the coarser microstructure (Figs. 2a, b) as well as the smaller line broadening observed from the upper side as compared to the wheel side.

5. Conclusions

(1) Both the hypo-eutectic alloys and the hyper-eutectic alloys show a thin "featureless" zone at the wheel side. On top of this zone a dendritic region of columnar grains is observed for the hypo-eutectic alloys, whereas a region showing a facetted growth is observed for the hyper-eutectic alloys.

(2) In the hypo-eutectic alloys the aluminium-rich phase at the wheel side shows a preferred orientation different from the one at the upper side, whereas the silicon-rich phase is randomly oriented. In the hyper-eutectic alloy no significant texture is observed.

(3) The silicon-rich phase at the wheel side has a larger microstrain and a smaller domain size than at the upper side, which is presumably due to the difference in cooling rate between both sides.

(4) A larger circumferential velocity of the rotating wheel is accompanied by a larger cooling and solidification rate and thus "broadens" the texture, decreases the domain size and enlarges the microstrain.

Acknowledgement

The authors are indebted to P. F. Colijn and D. Nelemans for their skilful assistance with optical and scanning electron microscopy.

References

1. L. KATGERMAN, H. KLEINJAN, R. W. E. KROPF and W. E. ZALM, in "Proceedings of the 2nd Inter-National Symposium: Materials and Energy from Refuse" (MER2), edited by A. Buekens (KVIV, Antwerp, Belgium, 1981) p. 5.7.
2. A. BENDIJK, R. DELHEZ, L. KATGERMAN, TH. H. DE KEIJSER, E. J. MITTEMEIJER and N. M. VAN DER PERS, *J. Mater. Sci.* **15** (1980) 2803.
3. L. G. SCHULZ, *J. Appl. Phys.* **20** (1949) 1030.
4. G. R. LOVE, Oak Ridge Technical Memorandum, ORNL-TM-2018 (Oak Ridge National Laboratory, Oak Ridge, USA, 1968).
5. D. DELHEZ and E. J. MITTEMEIJER, *J. Appl. Cryst.* **15** (1982) 308.
6. R. DELHEZ, TH. H. DE KEIJSER, E. J. MITTE-MEIJER and N. M. VAN DER PERS, in "Proceed-ings of the Conference on Applied Crystallography", Kozubnik, Poland, August (1978), Vol. 1, edited by Z. Bojarski and T. Bold (Silesian University of Katowice and Institute of Ferrous Metallurgy in Gliwice, Katowice, Poland, 1979) p. 323.
7. TH. H. DE KEIJSER, J. I. LANGFORD, E. J. MITTEMEIJER and A. B. P. VOGELS, *J. Appl. Cryst.* **15** (1982) 308.
8. H. P. KLUG and L. E. ALEXANDER, "X-ray diffrac-tion procedures" (Wiley, New York, 1974).
9. R. K. NANDI and S. P. SEN GUPTA, *J. Appl. Cryst.* **11** (1978) 6.
10. T. R. ANANTHARAMAN, P. RAMACHANDRA-RAO, C. SURYANARAYAMA, S. LELE and K. CHATTOPADHYAY, *Trans. Ind. Inst. Met.* **30** (1977) 423.
11. M. COHEN, in "Proceedings of the 2nd International Conference on Rapid Solidification Processing: Principles and Technologies", Reston, Virginia, USA, March (1980), edited by R. Mehrabian, B. H. Kear and M. Cohen (Claitor's, Baton Rouge, 1980) p. 1.
12. H. JONES, *Rep. Prog. Phys.* **36** (1973) 1425.
13. H. JONES, in "Vacancies '76", edited by R. E. Smallman and J. E. Harris (The Metals Society, London, 1977) p. 175.
14. A. KIRIN and A. BONEFACIC, *J. Phys. F* **4** (1974) 1608.
15. E. J. MITTEMEIJER, R. DELHEZ, R. VAN ROOIJEN and W. HOYER, *J. Crystal Growth* **36** (1976) 249.
16. H. A. DAVIES, N. SHOHOJI and D. H. WARRING-TON, in "Proceedings of the 2nd International Conference on Rapid Solidification Processing: Principles and Technologies", Reston, Virginia, USA, March (1980), edited by R. Mehrabian, B. H. Kear and M. Cohen (Claitor's, Baton Rouge, 1980) p. 153.
17. G. WASSERMAN and J. GREWEN, "Texturen metallischer Werkstoffe", 2nd edn. (Springer-Verlag, Berlin, 1962).
18. E. J. MITTEMEIJER, P. VAN MOURIK and TH. H. DE KEIJSER, *Phil. Mag.* **A43** (1981) 1157.
19. E. J. MITTEMEIJER and R. DELHEZ, in "Proceed-ings of the National Bureau of Standards Conference: Accuracy in Powder Diffraction", Gaithersburg, Maryland, June (1979), NBS Special Publication 567, edited by S. Block and C. R. Hubbard (US Department of Commerce, National Bureau of Standards, Washington, D.C., 1980) p. 271.

Received 30 November 1981
and accepted 1 March 1982